Clinical Ophthalmology

Dovepress
open access to scientific and medical research

Open Access Full Text Article

ORIGINAL RESEARCH

Interactive navigation-guided ophthalmic plastic surgery: assessment of optical versus electromagnetic modes and role of dynamic reference frame location using navigation-enabled human skulls

This article was published in the following Dove Press journal:
Clinical Ophthalmology
25 November 2016
Number of times this article has been viewed

Mohammad Javed Ali[1]
Milind N Naik[1]
Chetan Mallikarjuniah Girish[1]
Mohammad Hasnat Ali[2]
Swathi Kaliki[2]
Tarjani Vivek Dave[1]
Gautam Dendukuri[1]

[1]Ophthalmic Plastic Surgery Service, [2]The Operation Eyesight Universal Institute for Eye Cancer, L.V. Prasad Eye Institute, Hyderabad, India

Aim: The aim of this study was to assess the anatomical accuracy of navigation technology in localizing defined anatomic landmarks within the orbit with respect to type of technology (optical versus electromagnetic systems) and position of the dynamic reference marker on the skull (vertex, temporal, parietal, and mastoid) using in vitro navigation-enabled human skulls. The role of this model as a possible learning tool for anatomicoradiological correlations was also assessed.

Methods: Computed tomography (CT) scans were performed on three cadaveric human skulls using the standard image-guidance acquisition protocols. Thirty-five anatomical landmarks were identified for stereotactic navigation using the image-guided StealthStation S7™ in both electromagnetic and optical modes. Three outcome measures studied were accuracy of anatomical localization and its repeatability, comparisons between the electromagnetic and optical modes in assessing radiological accuracy, and the efficacy of dynamic reference frame (DRF) at different locations on the skull.

Results: The geometric localization of all the identified anatomical landmarks could be achieved accurately. The Cohen's kappa agreements between the surgeons were found to be perfect (kappa =0.941) at all predetermined points. There was no difference in anatomical localization between the optical and electromagnetic modes ($P \leq 0.001$). Precision for radiological identification did not differ with various positions of the DRF. Skulls with intact anatomical details and careful CT image acquisitions were found to be stereotactically useful.

Conclusion: Accuracy of anatomic localization within the orbit with navigation technology is equal with optical and electromagnetic system. The location of DRF does not affect the accuracy. Navigation-enabled skull models can be potentially useful as teaching tools for achieving the accurate radiological orientation of orbital and periorbital structures.

Keywords: navigation, image guidance, orbit, anatomy, teaching model, ophthalmic plastic surgery

Introduction

Interactive navigation-guided surgeries are increasingly becoming versatile in ophthalmic plastic surgery.[1–5] Enhanced precision and safety, intraoperative positional and spatial orientation, and minimizing potential complications are the major benefits of stereotactic surgeries.[1–5] Preoperative conventional plaster models are popular in

Correspondence: Milind N Naik
Ophthalmic Plastic Surgery Service, L.V. Prasad Eye Institute, Hyderabad 500001, India
Email milind@drmilindnaik.com

submit your manuscript | www.dovepress.com
Dovepress
http://dx.doi.org/10.2147/OPTH.S118079

craniomaxillofacial surgeries for better planning of subsequent complex surgeries. In recent times the stereolithographic models and 3D printed models have also been used to simulate pathologies and to plan and practice before the actual surgery.[6–9] Virtual planning of surgeries is increasingly gaining foothold in maxillofacial and endoscopic skull base surgeries.[10–12] In this context, it is also important to use this technology for learning anatomicoradiological correlations in vitro and for training to perform subsequent intraoperative navigation with ease and confidence. The authors of the present study report their preliminary experiences with using navigation-enabled human skulls for determining the efficacy of optical versus electromagnetic mode and the influence of dynamic reference frame (DRF) positions on the accuracy of navigation.

Methodology

Institutional Review Board approval of L.V. Prasad Eye Institute was obtained. As per Institutional guidelines patient consent was not needed. Computed tomography (CT) scans were performed on three cadaveric human skulls using the standard image-guidance acquisition protocols (Figure 1A). The skulls were stabilized on the CT table and contiguous CT scans of 1 mm thickness were performed from the inferior aspect of the horizontal portion of alveolar processes up to the vertex. Thirty-five bony anatomical landmarks (7 major bony surfaces, 13 fissures and foramina, 8 suture lines, and 7 lacrimal landmarks) were identified for stereotactic navigation (Table 1). The navigation was performed using the image-guided StealthStation S7™ system (Medtronic, Minneapolis, MN, USA) in the optical mode and electromagnetic mode using the AxiEM™ technology. Registration process for the skulls was completed using the trace (Figure 1B). Apart from the routine navigation probes, a malleable neuronavigation shunt probe (Figure 1C) was used for assessing the fissures and foramina. 3D models of the navigation-enabled skulls were simultaneously used during radiological identification of the geometric landmarks. The four-panel window of the StealthStation S7 system was designed in a way to include CT scans in any two chosen planes along with the anatomical skull and 3D reconstruction of the skull, so that a single desired landmark could be displayed simultaneously in multiple ways to enhance learning. Accuracy of anatomical localization, help with radiological orientation in all the CT planes, and repeatability of localization were assessed by two consultants experienced with navigation techniques. The accuracy was defined as excellent when the two points exactly matched, good when the radiologic point deviated within 2 mm of that on the cadaver skull, acceptable when the radiologic point deviated between 3 and 5 mm of that on the cadaver skull, and

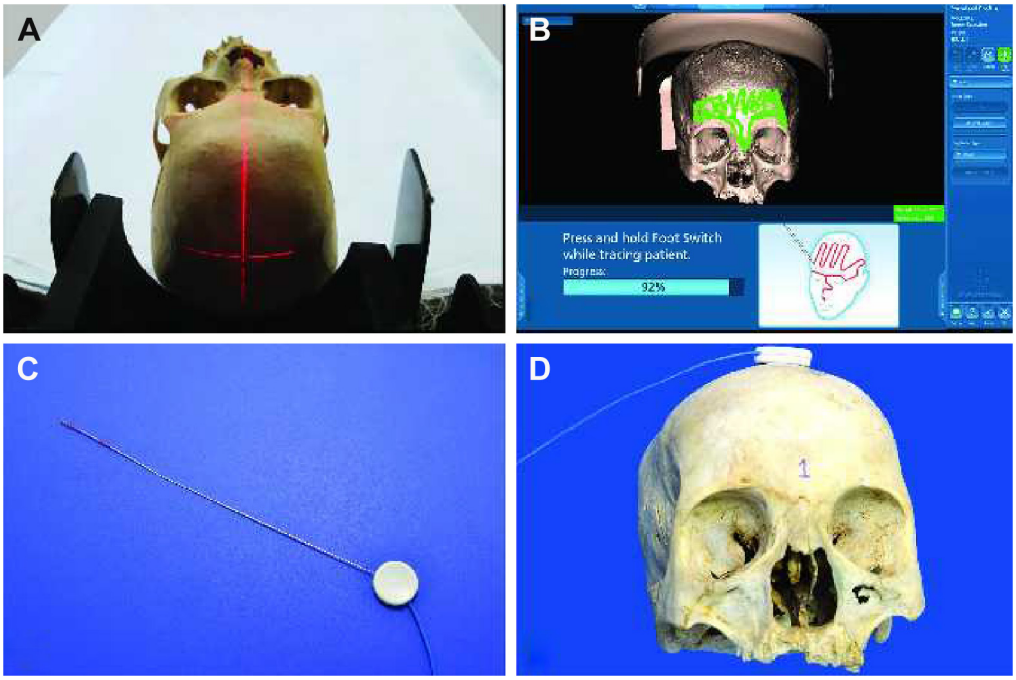

Figure 1 Techniques in navigation enabling of human cadaveric skulls.
Notes: External photograph showing computed tomography acquisition of the skulls as per standard navigation protocols (**A**). Navigation registration of the skull with the trace method (**B**). Neuronavigation-enabled shunt probe (**C**). Skull model with dynamic reference frame at the vertex (**D**).

Table 1 Navigation-enabled skull models – periocular anatomical landmarks

Accuracy grading	CON1	CON2
I. Major bony surfaces (gross radiological localization of bones)		
1. Orbital plate of frontal bone	E^{OP}, E^{EM}	E^{OP}, E^{EM}
2. Orbital plate of ethmoid bone	E^{OP}, E^{EM}	E^{OP}, E^{EM}
3. Orbital plate of maxillary bone	E^{OP}, E^{EM}	E^{OP}, E^{EM}
4. Orbital plate of zygomatic bone	E^{OP}, E^{EM}	E^{OP}, E^{EM}
5. Greater wing of the sphenoid	E^{OP}, E^{EM}	E^{OP}, E^{EM}
6. Lesser wing of the sphenoid	G^{OP}, G^{EM}	E^{OP}, E^{EM}
7. Lacrimal bone	E^{OP}, E^{EM}	E^{OP}, E^{EM}
II. Fissures and foramina		
1. Infraorbital foramen	E^{OP}, E^{EM}	E^{OP}, E^{EM}
2. Supraorbital foramen	E^{OP}, E^{EM}	E^{OP}, E^{EM}
3. Anterior end of infraorbital groove	G^{OP}, G^{EM}	G^{OP}, G^{EM}
4. Posterior end of infraorbital groove	G^{OP}, G^{EM}	G^{OP}, G^{EM}
5. Anterior end of inferior orbital fissure	G^{OP}, G^{EM}	G^{OP}, G^{EM}
6. Posterior end of inferior orbital fissure	G^{OP}, G^{EM}	G^{OP}, G^{EM}
7. Inferior end of superior orbital fissure	E^{OP}, E^{EM}	E^{OP}, E^{EM}
8. Superior end of superior orbital fissure	E^{OP}, E^{EM}	E^{OP}, E^{EM}
9. Optic foramen – medial and lateral end	E^{OP}, E^{EM}	E^{OP}, E^{EM}
10. Optic canal	E^{OP}, E^{EM}	E^{OP}, E^{EM}
11. Posterior ethmoidal foramen	G^{OP}, G^{EM}	G^{OP}, G^{EM}
12. Accessory anterior ethmoidal foramen (if present)	G^{OP}, G^{EM}	G^{OP}, G^{EM}
13. Anterior ethmoidal foramen	E^{OP}, E^{EM}	E^{OP}, E^{EM}
III. Suture lines		
1. Nasofrontal suture	G^{OP}, G^{EM}	G^{OP}, G^{EM}
2. Frontomaxillary suture	G^{OP}, G^{EM}	G^{OP}, G^{EM}
3. Zygomaticomaxillary suture	G^{OP}, G^{EM}	G^{OP}, G^{EM}
4. Frontozygomatic suture	E^{OP}, E^{EM}	E^{OP}, E^{EM}
5. Sphenofrontal suture	G^{OP}, G^{EM}	G^{OP}, G^{EM}
6. Lacrimomaxillary suture	G^{OP}, G^{EM}	G^{OP}, G^{EM}
7. Lacrimoethmoid suture	G^{OP}, G^{EM}	G^{OP}, G^{EM}
8. Sutura notha	G^{OP}, G^{EM}	G^{OP}, G^{EM}
IV. Major lacrimal landmarks		
1. Anterior lacrimal crest	E^{OP}, E^{EM}	E^{OP}, E^{EM}
2. Posterior lacrimal crest	E^{OP}, E^{EM}	E^{OP}, E^{EM}
3. Upper end of lacrimal fossa	E^{OP}, E^{EM}	E^{OP}, E^{EM}
4. Mid lacrimal fossa	E^{OP}, E^{EM}	E^{OP}, E^{EM}
5. Lower lacrimal fossa	E^{OP}, E^{EM}	E^{OP}, E^{EM}
6. Bony nasolacrimal duct entrance – anterior and posterior ends	G^{OP}, G^{EM}	G^{OP}, G^{EM}
7. Transnasal identification of the bony lacrimal fossa	E^{OP}, E^{EM}	E^{OP}, E^{EM}

Abbreviations: E, excellent; EM, electromagnetic mode; G, good; OP, optical mode; CON, consultant.

poor when the radiologic point deviated more than 5 mm of that on the cadaver skull (Table 1). Landmark localization was repeated three times for each of the parameters. Comparisons were performed between the electromagnetic (Figure 1D) and optical modes (Figure 2A) in assessing radiological localization. The DRF in the electromagnetic mode was placed at different locations (vertex, frontoparietal suture, pterions, and mastoid) and its efficacy in radiological localization was studied (Figures 1D and 2B–D). Statistical analysis was performed using the Cohen's kappa agreements and values of 0.8–1 were determined to be a perfect agreement. A *P*-value of <0.05 was considered significant.

Results

Anatomicoradiological correlations

The geometric localization of all the identified anatomical landmarks could be achieved accurately. However, it was noted that in order of ease and accuracy, major bony surfaces could be easily and quickly localized (Figure 3) followed by lacrimal landmarks, fissures, foramina, and sutures. This was reflected by the grading scores for each landmark as depicted in Table 1. Point localization of the lateral and medial ends of bony entrances like the nasolacrimal canal and optic canal could be meticulously studied. Precise positional information could be obtained in real time in canals, fissures, and grooves as the probe traverses from one anatomical end to another (Figures 4A, B and 5). Although the localization of sutures was exact, the radiological details in terms of morphology could not be appreciated and this could partly be explained by the postmortem changes in skull tissues following prolonged preservation (Figure 6). The radiological orientation and anatomicoradiological correlations could be assessed in all cases by the consultants with accurate repeatability. The kappa agreement value between the consultants for the predetermined anatomical points was 0.941 for optical and electromagnetic modes. The four-panel window of the StealthStation S7 system incorporating the anatomical skull navigation, CT scans, and 3D reconstruction facilitated learning from all the perspectives for a desired landmark (Figures 3–6).

Optical versus the electromagnetic mode

There was no difference in anatomical localization between the optical and electromagnetic modes ($P<0.001$). However, the fissures and foramina could be easily located using the neuronavigation shunt probe as compared with the regular navigation probes and this was facilitated by its slender design and malleability (Figure 1C). The electromagnetic mode using the AxiEM technology was found to be easier to set up because it does not need securing any separate head frame (Figure 1D) unlike in the optical mode (Figure 2A).

Positional variations of DRF

Precision for radiological identification did not vary with variations in the positions of the DRF (Figures 1D and 2B–D). However, it was found that the registration process becomes more relevant when the DRF is placed on the mastoid bone. This essentially means that as the DRF moves away

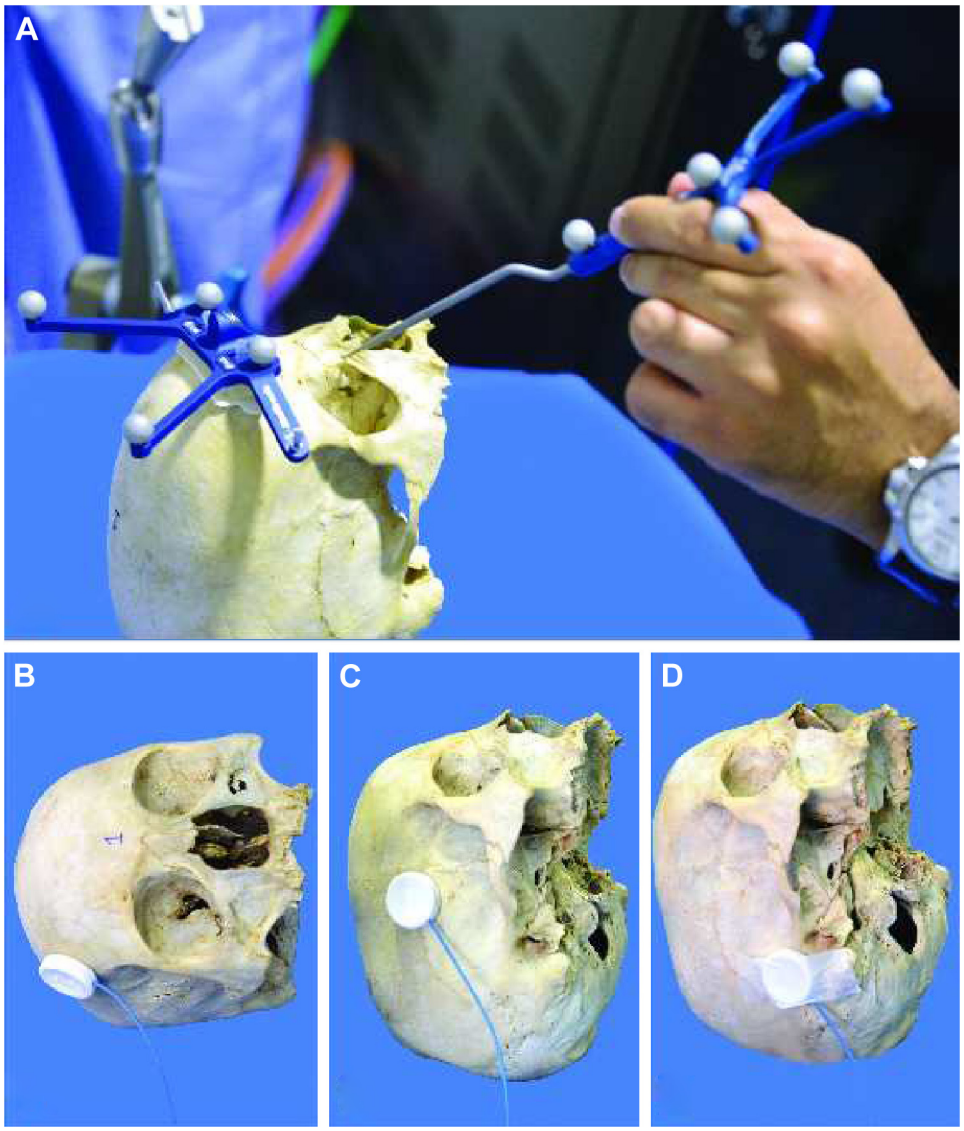

Figure 2 Techniques in navigation enabling of human cadaveric skulls.
Notes: External photographs of the skulls showing the optically enabled model with head frame (**A**) and various positions of the dynamic reference frame at superior frontoparietal suture (**B**), pterions (**C**), and mastoid (**D**).

from the periorbital region, the registration process should be meticulous with as few as possible "in-air points" or areas of registration discontinuity.

Discussion

The current study reports the techniques of developing navigation-enabled human skulls and utilizing them as models for learning accurate anatomicoradiological localization of orbital and periorbital bony landmarks. In vitro learning using such models would help surgeons to orient themselves radiologically and use intraoperative navigation with ease during orbital surgeries. This study also concluded that there is no significant difference with use of either optical or electromagnetic modes and the position of DRF does not influence the accuracy of navigation.

3D models and stereolithography have been shown to provide an opportunity to the surgeon to practice and navigate the desired anatomy of a patient before the actual surgery. Ritacco et al[10] proposed a validation method to compare virtual planned trajectory with the real executed course and found that the surgical models enhance the safety and accuracy of surgeons while performing on patients. Novelli et al[12] showed encouraging results in their series of 11 patients of combined orbital wall and zygoma injuries. They proposed integration of surgical navigation with stereolithographic models to tailor the reconstruction to individual patients.

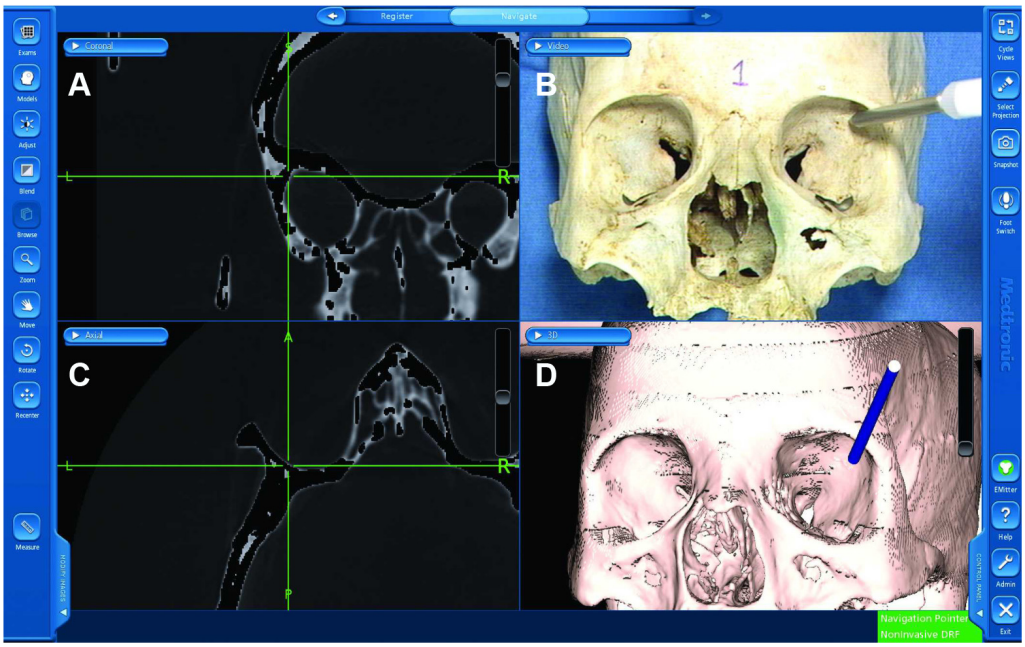

Figure 3 Four-window active navigation image showing the localization of the greater wing of the sphenoid.
Notes: Note the computed tomography images (**A**, **C**), the anatomical skull model (**B**), and the 3D reconstruction of the same cadaveric skull (**D**).
Abbreviations: L, left; R, right; DRF, dynamic reference frame.

They showed that it was possible to reconstruct volume of the fractured orbit to that of a healthy orbit with good clinical outcomes. Dallan et al[13] performed quantification of surgical freedom on cadaver heads using the magnetic navigation control system. They found that surgical freedom for any given point is a good tool for comparing different surgical approaches and navigation models can help in deciphering this.

The current in vitro study has significant surgical relevance apart from anatomical learning. Practice with navigation-enabled skulls can enhance the surgeons' adaptability to assess precisely their geometric locations

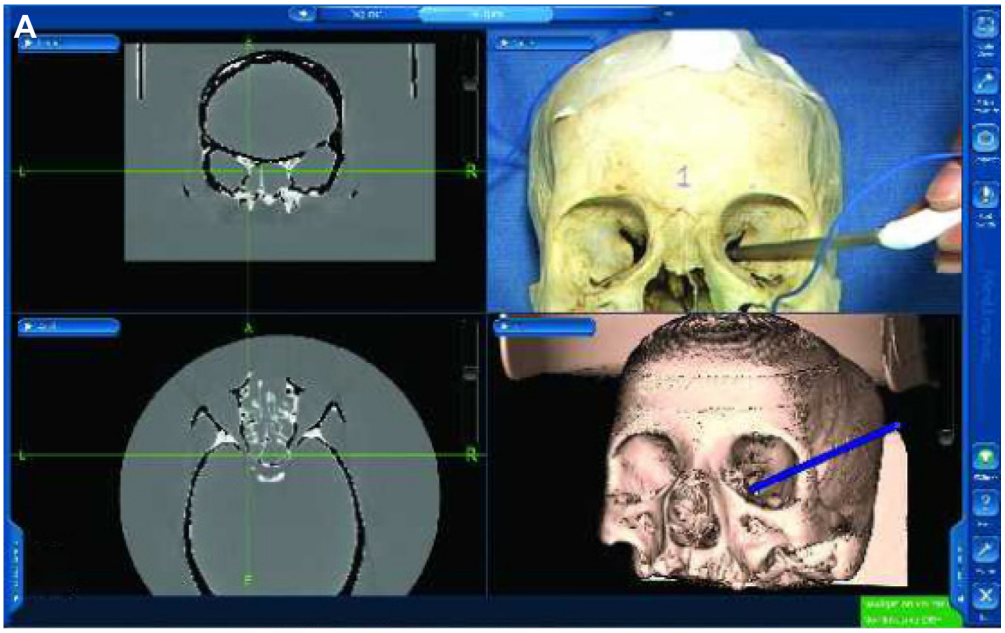

Figure 4 (*Continued*)

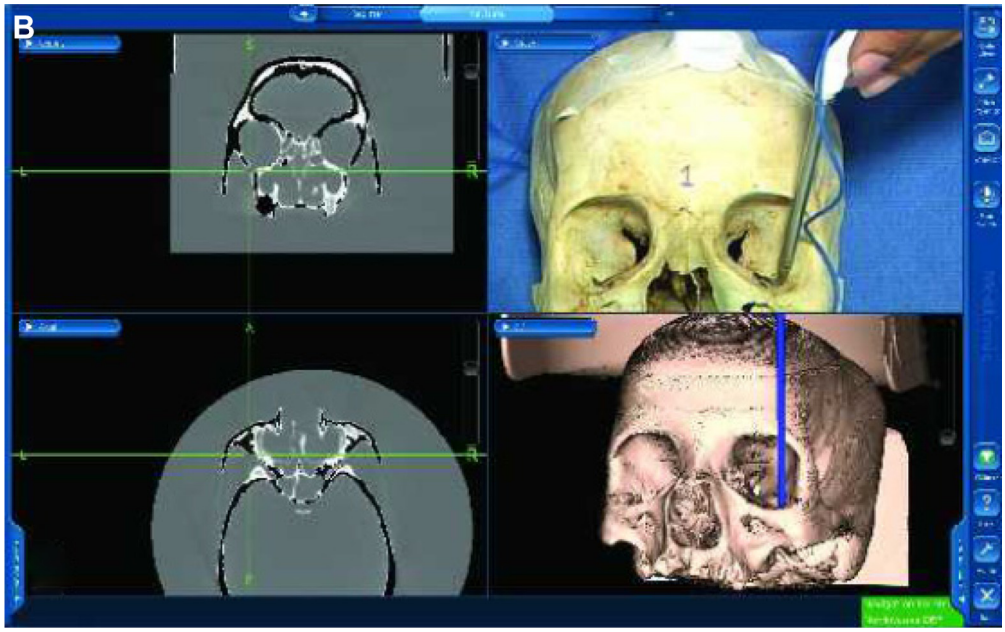

Figure 4 Active navigation of the orbital fissures.
Notes: Four-window active navigation image showing localization of the inferior end of superior orbital fissure (**A**) and anterior end of inferior orbital fissure (**B**).
Abbreviations: L, left; R, right; DRF, dynamic reference frame.

intraoperatively and would also help them to take into account the adjacent crucial radiological landmarks during surgeries. The present study showed that the malleable neuronavigation shunt probe was more useful for assessing the localization of foramina and hence has a potential application while navigating narrow orbital confines during surgeries. The current study did not show any difference in accuracy with either electromagnetic or optical navigation modality; however, it may not be possible to entirely extrapolate this finding to live orbital surgeries and the choice of navigation can still be debated.[5,8,10] As optical mode has a problem with "line of sight" interference, this can be a potential limiting factor while operating with assistance in the periorbital area. In this context, using the AxiEM electromagnetic mode is

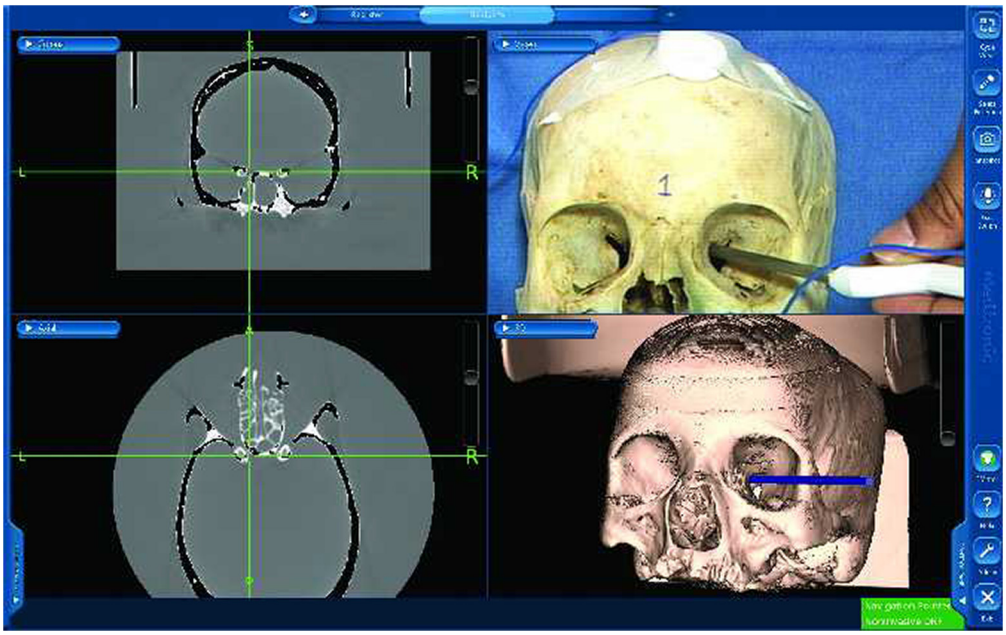

Figure 5 Active navigation of the optic canal.
Note: Four-window active navigation image showing the probe tracking within the optic canal.
Abbreviations: L, left; R, right; DRF, dynamic reference frame.

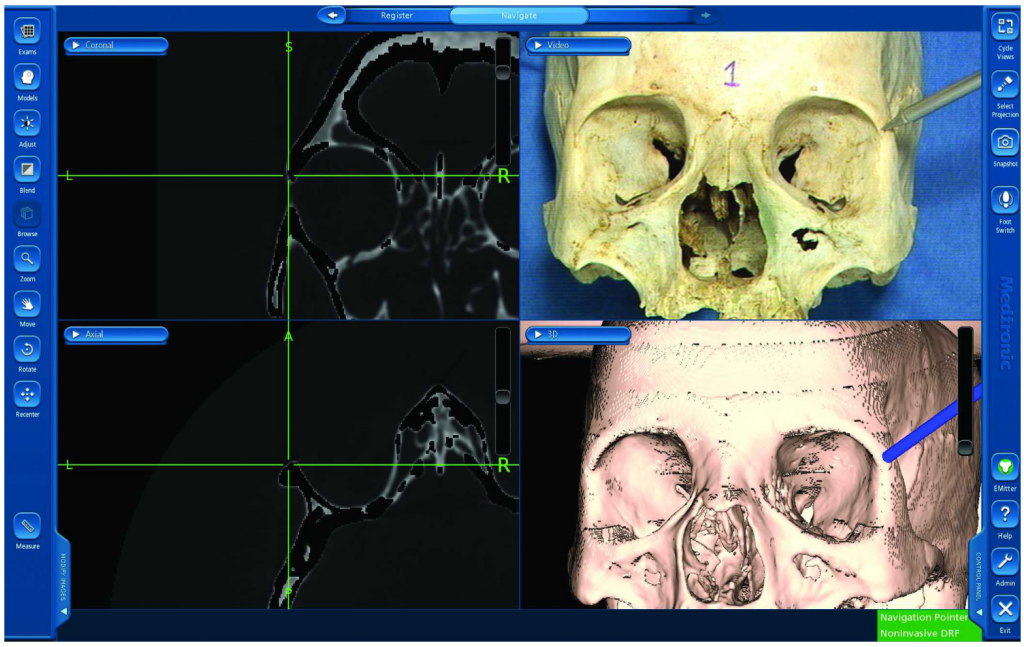

Figure 6 Active navigation of the sutures.
Note: Four-window active navigation image showing localization of the frontozygomatic suture.
Abbreviations: L, left; R, right; DRF, dynamic reference frame.

perhaps less cumbersome because it eliminates the need for securing a headband in the perioperative area. The current study also answered a crucial question with regard to the placement of DRF. There was no difference in accurate localization of anatomical landmarks, irrespective of the location of DRF. However, it is very important to achieve a very good registration with minimal "in-air" points when the DRF is at the mastoid. This finding essentially means that the DRF can be placed at a convenient location where it does not interfere with the surgical field and hence can keep the surgeon free from intraoperative navigation disruptions.

The navigation-enabled skull models along with their CT acquisition data can be transported to any desired location where other navigation machines are available and can be used to train people at multiple locations. Subsequently, it would be useful to study the differences and compare between a simulation system and the real operative scenarios and also the learning curves between surgeons with different levels of experience. The limitations of this study include failure to account for racial variations in anatomy and problems with acquiring desired density images in bony windows secondary to postmortem skeletal changes over a period of time.

In conclusion, navigation-enabled skull models can be very useful teaching tools for achieving the accurate radiological orientation of orbital and periorbital structures. Such in vitro learning could facilitate subsequent surgical planning and intraoperative navigation in ophthalmic plastic surgeries.

Acknowledgments

Mohammad Javed Ali receives royalties from Springer for his textbook *Principles and Practice of Lacrimal Surgery*. Support is provided by "The Operation Eyesight Universal Institute for Eye Cancer" (SK), Hyderabad, India. The funders had no role in the preparation, review, or approval of the manuscript.

Disclosure

The authors report no conflicts of interest in this work.

References

1. Servat JJ, Elia MD, Gong D, Manes RP, Black EH, Levin F. Image-guided orbital decompression: techniques, principles and preliminary experience with 6 consecutive cases. *Orbit*. 2014;33(6):433–436.
2. Karcioglu ZA, Mascott CR. Computer-assisted image-guided orbit surgery. *Eur J Ophthalmol*. 2006;16(3):446–452.
3. Campbell AA, Grob SR, Yoon MK. Novel surgical approaches to the orbit. *Middle East Afr J Ophthalmol*. 2015;22(4):435–441.
4. Terpolilli NA, Rachinger W, Kunz M, et al. Orbit-associated tumours: navigation and control of resection using computed tomography. *J Neurosurg*. 2016;124(5):1319–1327.
5. Ali MJ, Naik MN . Image-guided dacryolocalization (IGDL) in traumatic secondary acquired lacrimal duct obstructions (SALDO). *Ophthal Plast Reconstr Surg*. 2015;31(5):406–409.
6. Narayanan V, Narayanan P, Rajagopalan R, et al. Endoscopic skull base training using 3D printed models with pre-existing pathology. *Eur Arch Otorhinolaryngol*. 2015;272(3):753–757.

7. Waran V, Pancharatnam D, Thambinayagam HC, et al. The utilization of cranial models created using rapid prototyping techniques in the development of models for navigation training. *J Neurol Surg A Cent Eur Neurosurg*. 2014;75(1):12–15.
8. Berger M, Kallus S, Nova I, et al. Approach to intraoperative electromagnetic navigation in orthognathic surgery: a phantom skull based trial. *J Craniomaxillofac Surg*. 2015;43(9):1731–1736.
9. Kang SH, Lee JW, Lim SH, Kim YH, Kim MK. Verification of the usability of a navigation method in dental implant surgery: in-vitro comparison with the stereolithographic surgical guide template method. *J Craniomaxillofac Surg*. 2014;42(7):1530–1535.
10. Ritacco LE, Di Lella F, Mancino A, Gonzalez Bernaldo de Quiros F, Boccio C, Milano FE. 3D printed models and navigation for skull base surgery: case report and virtual validation. *Stud Health Technol Inform*. 2015;216:1025.
11. Adolphs N, Haberl EJ, Liu W, Keeve E, Menneking H, Hoffmeister B. Virtual planning for craniomaxillofacial surgery – 7 years of experience. *J Craniomaxillafac Surg*. 2014;42(5):e289–e295.
12. Novelli G, Tonellini G, Mazzoleni F, Bozzetti A, Sozzi D. Virtual surgery simulation in orbital wall reconstruction: integration of surgical navigation and stereolithographic models. *J Craniomaxillofac Surg*. 2014;42(8):2025–2034.
13. Dallan I, Lenzi R, de Notaris M, et al. Quantitative study on endoscopic endonasal approach to the posterior sino-orbito-cranial interface: implications and clinical considerations. *Eur Arch Otolaryngol*. 2014;271(8):2197–2203.